

Mössbauer studies with I^{131} and I^{125} sources implanted in iron

H. de Waard* and R. L. Cohen

Bell Laboratories, Murray Hill, New Jersey 07974

S. R. Reintsema and S. A. Drentje

Laboratorium voor Algemene Natuurkunde, University of Groningen, Groningen, Netherlands

(Received 14 May 1974)

Using implanted sources of I^{131} and I^{125} in iron, the hyperfine (hf) fields and recoilless fractions of the daughter nuclei, Xe^{131} and Te^{125} , respectively, have been investigated by means of the Mössbauer effect of their first-excited-state γ transitions. In both cases, the Mössbauer spectra consist of different components, indicating that the implanted atoms occupy a number of inequivalent sites. We performed measurements at different temperatures to deduce recoilless fractions for the observed components and the relative occupations of the different sites. The data for both cases have been fitted with a model that assumes three different hf spectral components, identified as having high (h), intermediate (i) and low (l) hf fields. For $Fe\ Xe^{131}$, values $B_{hf}^{(h)} = 1.55 \pm 0.10$ MG, $B_{hf}^{(i)} = 1.16 \pm 0.15$ MG, and $B_{hf}^{(l)} = 0.3 \pm 0.1$ MG were found; for $Fe\ Te^{125}$: $B_{hf}^{(h)} = 681 \pm 4$ kG, $B_{hf}^{(i)} = 540 \pm 15$ kG, and $B_{hf}^{(l)} = 190 \pm 60$ kG. In agreement with channeling results, the h component is ascribed to Xe or Te atoms in substitutional sites. A calculation of hf fields for various defect clusters makes it probable that the i component corresponds to impurity atoms associated with one vacancy in a nearest-neighbor position. The l component is not sharply defined; it is assumed to correspond to several different vacancy clusters, consisting of an impurity atom associated with two or more vacancies.

I. INTRODUCTION

In recent years the amount of information on magnetic hyperfine (hf) fields of dilute impurities in magnetic metals has been growing rapidly. The information is important both for a better understanding of the origin of the fields and for nuclear-physics experiments in which these fields are used for the measurements of magnetic moments of short-lived nuclear states. Measurements of hf structure by spectroscopic techniques also provide information on the existence and population of different sites for the impurity ions.

Four techniques have been widely used for embedding impurities in magnetic hosts for hf studies. The two traditional techniques, melting the host and impurity together and diffusion, can only be used when the impurity forms a solid solution with the host, and this solid solution can be metastably retained at the measuring temperature. These techniques fail if the solubility of the impurity in the host is very low, or if the impurity reacts chemically with the host material. In these cases, the impurities can be introduced by implantation of energetic (10 keV–10 MeV) impurity ions into the host. Ions may acquire these energies either by the recoil from nuclear reactions or directly, using electrostatic acceleration.

Normally, samples produced by implantation techniques contain so few impurity atoms that it is not possible to study the hf interaction by nuclear-resonance or specific-heat techniques. Instead, radioactive ions have been implanted, and the

hyperfine interaction studied by means of its effects on the nuclear radiation emitted. Basically, there are three different techniques for measuring these effects. In the experimental work we report here, the hf splitting of the nuclear states is directly determined using Mössbauer spectroscopy to study the emitted γ rays. The second technique that has been used to determine the hf interactions of implanted radioactive nuclei is that of low-temperature nuclear orientation, in which the nuclear spin system is cooled to temperatures such that kT is of the order of the hf coupling energy. This results in a net nuclear orientation, which can be measured from the anisotropy of the emitted radiation. Finally, the rotation of γ -ray angular distributions resulting from the precession of the γ -emitting nuclei in the hf field may be measured [this is the perturbed-angular-correlation (PAC) technique].

To a certain extent, these three techniques are complementary, and information from all of them must be combined to obtain a systematic understanding of the origin of the hf fields. In this light, we should emphasize that while the nuclear-orientation experiments yield the hf interaction of the *parent* nucleus, the PAC technique measures the hf interaction of an excited state of the *daughter* nucleus. Mössbauer spectroscopy is the only technique from which information about the hf interaction of an excited state as well as the ground state of the daughter nucleus can be obtained. Thus, in many cases hf fields can be directly deduced from the ground-state nuclear moments, which

are usually well known.

In hf interaction measurements on implanted sources, complications often arise because not all implanted ions are in equivalent sites. This has been clearly shown by recent hf measurements and by back-scatter channeling measurements to determine lattice locations.

In some cases, e.g., $Sb(Z=51)^{1,2}$ and $Te(Z=52)^{3,4}$ implanted in iron, measurements indicate that all the impurities have the same hf field, and therefore are probably in the same sites. The substitutional character of these sites has been confirmed by channeling measurements.^{5,6} In other cases, e.g., $Xe(Z=54)$ implanted in iron,^{4,7} the complex structure of Cs^{133} Mössbauer spectra (obtained with $FeXe^{133}$ sources) demonstrates the existence of at least three different sites. These results have also been supplemented by channeling studies⁸ that show rather low substitutional fractions (0.3–0.5) for Xe in iron single crystals, implanted to doses comparable with those used for the Mössbauer measurements. The presence in implanted sources of sites with different hf fields seriously complicates the interpretation of nuclear-orientation and perturbed-angular-correlation measurements, which can usually be analyzed only in terms of one value of the hf field.

In this paper, we present results of new Mössbauer spectroscopy measurements on Xe^{131} in iron and Te^{125} in iron. The spectra for each of these systems show the presence of three different hf fields. The hf field results are discussed both in terms of a microscopic model of wave-function overlap between host and impurity, and systematics of hf fields for other ions. The sources for the two experiments were made by implanting I^{131} and I^{125} , respectively, into iron. The site populations and symmetries for the implanted I atoms are discussed in the light of the Mössbauer measurements on the daughter species. We have tried to bring together the results of a number of different hf and lattice-location measurements to construct as complete a picture as possible at this time of the results of implantation of the elements $Sb(Z=51)$ to $Cs(Z=55)$ into iron.

II. EXPERIMENTAL PROCEDURES

A. $FeXe^{131}$

Mössbauer investigations with xenon isotopes have been reported by Perlow *et al.*⁹ They mainly used the 40-keV transition in Xe^{129} ($T_{1/2} = 1$ nsec), fed in the decay of 1.6×10^7 -yr I^{129} . This transition was preferred over the 80-keV transition in Xe^{131} ($T_{1/2} = 0.5$ nsec), fed in the decay of 8-day I^{131} , because of its much higher recoilless fraction and its narrower linewidth. Only one measurement on the 80-keV transition, using a

$Na_2H_3I^{131}O_6$ source and a XeF_4 absorber, was carried out by Perlow.¹⁰ For our investigation we had to use I^{131} as the source activity because no usable implanted source can be made with the long-lived I^{129} activity.

Of the different absorber materials investigated by Perlow, sodium perxenate ($Na_4XeO_6 \cdot xH_2O$) has the largest recoilless fraction. Accordingly, we used a $Na_4XeO_6 \cdot 2H_2O$ absorber (Peninsular Chemical Research Inc., Gainesville, Fla.) of 18-mm diameter, containing 700 mg/cm² of the compound. Electronic processes absorb 60% of the incident 80-keV γ rays in this absorber. The absorber was tested with a 5-mCi source of $Na_2H_3I^{131}O_6$ (New England Nuclear) to determine its linewidth and resonance absorption. In the cryostat used for the first Xe^{131} experiments (carried out at Bell Labs), the absorber, immersed in liquid helium, is at 4.2 K, while the source, connected to the helium reservoir by copper braids is at a temperature of 8–10 K. Later experiments (at Groningen) were performed in a cryostat where the absorber was also in liquid helium but the source was contained in a small vacuum chamber immersed in the liquid. Its temperature could be varied from 4 to 120 K with the aid of a temperature-controlled heater. Strong sources are needed because only 5% of the I^{131} decay feeds the 80-keV transitions. The presence of a 364-keV line 20 times more intense than the 80-keV line necessitates the use of a planar germanium detector with optimum pulse shaping and careful collimation of the γ rays to minimize the background under the 80-keV line. Counting rates in the 80-keV channel between 1 and 5 kHz were obtained, with photopeak-to-background intensity ratios ranging from 1:0.8 to 1:2.

A background-corrected absorption effect $I_0 = (1.0 \pm 0.2)\%$ was obtained with the paraperiodate test source and the sodium perxenate absorber. The error in the dip is almost entirely due to the inaccuracy of the background correction. The width of the Lorentzian line that fits the measured spectrum is $\Gamma = 9.5 \pm 1$ mm/sec. The increase over the natural linewidth $\Gamma_0 = 6.8$ mm/sec probably arises largely from an unresolved quadrupole splitting in the source. Under this assumption, we should correct the measured absorption dip by a factor Γ/Γ_0 , which yields $I'_0 = 0.014 \pm 0.0032$. Since the interatomic distances and the crystal structure of the paraperiodate and the perxenate are very similar,¹¹ it appears reasonable to assume that the source and absorber recoilless fractions are not very different. Assuming them to be equal, a value $f(0) = 0.049 \pm 0.007$ is found for the recoilless fraction at $T = 0$ by solving the equation

$$I'_0 = f_0 \left\{ 1 - e^{-f(0)n_a\sigma_a/2} J_0 \left[\frac{1}{2} \text{if}(0)n_a\sigma_a \right] \right\}$$

for the line intensity,¹² using $n_a\sigma_a = 15.4$ (n_a is the

number of Xe^{131} atoms/cm² in the absorber, σ_a the resonant cross section of the 80-keV level). If the effect of line broadening due to absorber thickness is taken into account in the argument just presented, a slightly smaller value, $f(0) = 0.047 \pm 0.007$, is found. This corresponds to a characteristic temperature $\Theta_M \approx 150$ K. From this value of $f(0)$, a value for the $T = 0$ recoilless fraction $f(0)^{(40)}$ of the 40-keV transition of Xe^{129} in a perxenate absorber can be derived; $f(0)^{(40)} = 0.47 \pm 0.02$ in good agreement with the value given by Perlow.⁹

The Fe^{131} sources were made by implantation of I^{131} ions accelerated to 110 keV, each into three 30- μ -thick 99.999%-pure iron foils (held at room temperature) with the isotope separator of the Natuurkundig Laboratorium, Groningen, Netherlands. The sources were not heated after the implantation. Source strengths of 6.3 and 14.4 mCi were obtained starting from a 100-mCi sample in the ion source consisting of NaI^{131} in 5-mg NaI carrier. Because of the high specific activity of the starting material and because there is a mass difference of four units between the only stable iodine isotope (I^{127}) and the radioactive implanted isotope, the dose of stable iodine in the implanted source was relatively small. It is estimated at less than $4 \times 10^{14}/\text{cm}^2$, the initial I^{131} dose being $1 \times 10^{14}/\text{cm}^2$ for the first source and $2.3 \times 10^{14}/\text{cm}^2$ for the second source.

B. FeTe^{125}

The Te^{125} source preparations and experiments were carried out at Groningen. The 35.6-keV level of Te^{125} ($T_{1/2} = 1.6$ nsec) is fed both in the decay of 2.7γ Sb^{125} and of 60-day I^{125} . Mössbauer spectra of the 35.6-keV transition were measured both with a diffused FeSb^{125} source and an implanted FeI^{125} source.

The Sb^{125} activity, obtained as a carrier-free solution of SbCl_3 in HCl , was precipitated as Sb_2O_3 after addition of 2-mg SbCl_3 carrier. The oxide was reduced at 600 °C in a hydrogen stream and the metal vapor condensed in a quartz tube containing a 100-mg iron foil. The tube was subsequently evacuated and sealed at both ends. The antimony was then diffused into the iron at 800 °C for 5 h. In this way, a 400- μ Ci FeSb source containing 1% Sb was obtained.

The FeI^{125} source was implanted at an ion energy of 120 keV using 25-mCi I^{125} in 6-mg NaI in the ion source. The total implanted iodine dose was about $10^{15}/\text{cm}^2$, the source strength 450 μ Ci. A 22-mg/cm² ZnTe absorber, enriched to 71% in Te^{125} , was used both for the measurements with the FeI^{125} and with the FeSb^{125} source. The measurements were carried out in a liquid-helium cryostat in which both source and absorber are immersed in the refrigerant. An intrinsic Ge detector was used

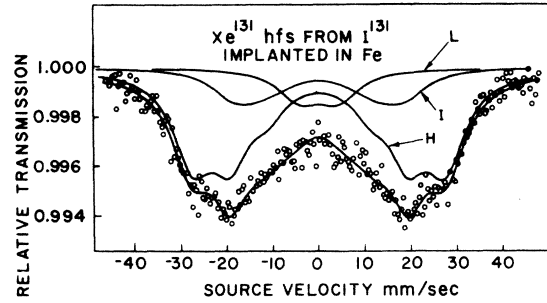


FIG. 1. Mössbauer spectrum obtained with implanted FeI^{131} source and Na_4XeO_6 absorber at liquid-helium temperature. The line drawn through the measured points represents a least-squares fit to a three-component model. Separate components are given by lines h (high field), i (intermediate field), and l (low field).

to measure the 35.6-keV line, which was completely resolved from the x rays accompanying the capture decay of I^{125} and the conversion of Te^{125} γ rays.

III. RESULTS AND MEASUREMENTS

A. FeXe^{131}

Mössbauer spectra of the 80-keV γ transition in Xe^{131} were recorded for source a , of strength 6.3 mCi, with source and absorber at liquid-helium and liquid-hydrogen temperatures and for source b , of strength 14.4 mCi, at 4.2, 40, 60, 80, and 115 °K while the absorber was kept at 4.2 °K. The result of a measurement with source a at liquid-helium temperature is shown in Fig. 1, that of a measurement with source b at 60 °K in Fig. 2. Because the spectrum is complex and incompletely resolved, an unambiguous analysis is only possible after giving some of the parameters fixed predetermined values. Under a pure magnetic hf interaction with hf field B_{hf} , the $I^* = \frac{1}{2} \rightarrow I = \frac{3}{2}$ 80-keV M_1 transition would be split into six Zeeman components with energies given by

$$E(m_g, m_e) = \mu_N B_{hf} (g_g m_g - g_e m_e),$$

$$m_g - m_e = 0, \pm 1.$$

Here, $g_g = 0.4606$ is the g factor and $m_g = -\frac{3}{2}, -\frac{1}{2}, +\frac{1}{2}, +\frac{3}{2}$ are the possible magnetic quantum numbers of the ground state; g_e and $m_e = -\frac{1}{2}, +\frac{1}{2}$ are the corresponding quantities for the 80-keV state and μ_N is the nuclear magneton. Normally the ratio g_e/g_g can be determined from Mössbauer hf spectra, but in this case the large linewidth and presence of inequivalent sites do not allow this.

Therefore, we have estimated the unknown g factor of the excited state from known magnetic-moment values of $\frac{1}{2}^+$ states in nearby even- Z nuclei. The $\frac{1}{2}^+$ ground state of Xe^{129} has $g_g = -1.5538$ and

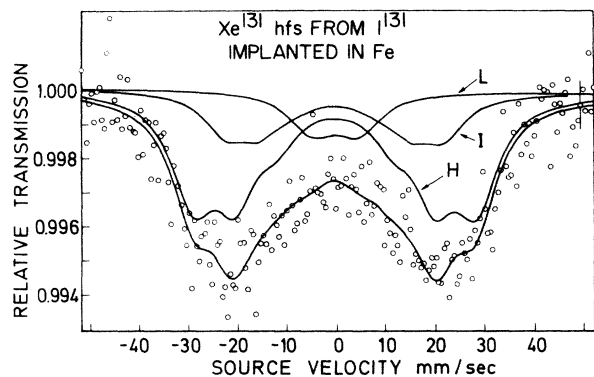


FIG. 2. Mössbauer spectrum obtained with implanted FeI^{131} source at 60 K and Na_4XeO_6 absorber at 4.2 K. The line drawn through the measured points represents a least-squares fit to the three-component model. Separate components are shown by lines *h* (high field), *i* (intermediate field), and *l* (low field). The resonance effect plotted here appears as large as that in Fig. 1 because the background under the γ -ray line is smaller, compensating for the reduced *f*.

an inspection of the $\frac{1}{2}^+$ states of three isotopes of $_{48}Cd$, four of $_{50}Sn$, and two of $_{52}Te$ shows that the absolute value of the *g* factor increases by amounts varying from 0.05 to 0.30 for each pair of neutrons added to a nucleus. We therefore consider $-1.55 > g_e > -1.9$ to be a range within which g_e should lie (corresponding to a range $-3.35 > g_e/g_g > -4.1$ for the *g*-factor ratio).

For the spin states, multipolarity, and *g* factors encountered here, the intensity ratios of the Zeeman components are given in order of increasing energy as $3:x:1:1:x:3$, where *x* depends on the angle between the magnetic hyperfine field and the direction of γ -ray emission. For hf fields oriented at random, $x=2$, while $x=4$ for complete orientation of the hf field perpendicular to the direction of γ emission. The $FeXe^{131}$ measurements were carried out without the use of an external field to magnetize the source, but, as is well known, near the surface of a foil, an appreciable magnetic alignment in the plane of the source foil is usually present. Earlier measurements on $FeTe^{127,13}$ using an unmagnetized source foil of the same thickness and the same iron, yielded a value $x > 2.5$ while our measurements on FeI^{125} and $FeSb^{125}$, to be described in Sec. III B carried out in a transverse field of 420 G, yielded $x \sim 2.7$. We therefore assume *x* to be in the range $2.5 < x < 3$ in the present case.

For predetermined values of g_e/g_g and *x* within the ranges just indicated, most of the measured spectra could not be least-squares fitted to a reasonable χ^2 value with less than three 6-line components, corresponding to three fractions *h*,

i, and *l* of the implanted atoms, with high, intermediate and low hyperfine magnetic fields. The symmetry of the spectra suggests that there is no appreciable quadrupole splitting and that the three components have about the same isomer shifts.

In all least squares fits we have given fixed values to the parameters g_e/g_g and *x* while one common isomer shift for all components and one common width for all lines were chosen as variable parameters. The hyperfine fields $B_{hf}^{(h,i,l)}$ and the relative intensities *I*(*h, i, l*) of each of the 3 components are further variable parameters for the measurements with source *a* and for the measurements at 4.2 and 40 K with source *b*. Fewer free parameters were chosen for the higher-temperature measurements with source *b* (at 60, 80, and 115 K), because of the reduced effect. In the analysis of these runs, the field(s) and the common linewidth were kept fixed at the average values resulting from the 4.2- and 40-K measurements. Moreover, only two components (*h* and *i*) were used at 80 K and only one (*h*) at 115 K.

All results have been summarized in Table I while in Fig. 3 results for source *a* are shown, obtained for several different values of the predetermined parameters *x* and g_e/g_g . The shaded regions give an indication of the correlation between field and intensity values that follows from the error matrix produced by the computer program. The centers of the ellipses give the fields and intensities for $x=2.7$ and $g_e/g_g=-3.74$, i. e., parameter values in the middle of the allowed regions. The circles, triangles, and squares cor-

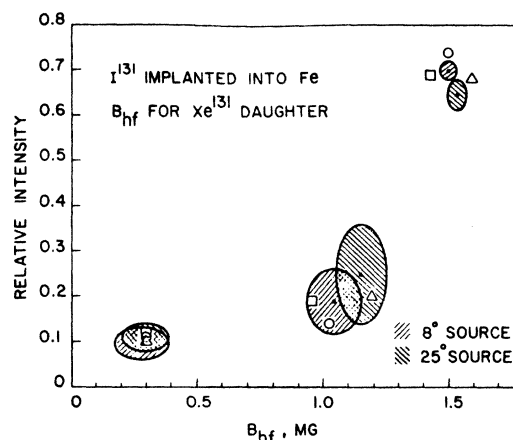


FIG. 3. Results for hyperfine magnetic fields B_{hf} and relative intensities with three-component model. The shaded ellipses represent the correlated errors for the case of midrange choices of the parameters *x* (for degree of source magnetization) and g_e/g_g (for *g*-factor ratio): $x=2.7$, $g_e/g_g=-3.74$. The squares are obtained for $x=2.7$, $g_e/g_g=-4.1$; the triangles for $x=2.7$, $g_e/g_g=-3.35$; and the circles for $x=3$, $g_e/g_g=-3.74$.

TABLE I. Parameters obtained from Mössbauer spectra of Fe^{131} sources vs Na_4XeO_6 absorber, using the 80.16-keV transition in Xe^{131} .

Source	Temperature (K)		Linewidth (mm/sec)	Isomer shift (mm/sec)	Component	Intensity ^a (I_0 , %) ^b	Hyperfine field ^a (B_{hf} , MG)
	Source	Absorber					
a	8	4.2	10 ± 1	0.0 ± 0.2	<i>h</i>	4.8 ± 0.5	1.51 ± 0.03
					<i>i</i>	1.3 ± 0.5	1.05 ± 0.14
					<i>l</i>	0.8 ± 0.3 ⁵	0.3 ± 0.1
	25	20.4	10 ± 1	0.0 ± 0.2	<i>h</i>	4.0 ± 0.4	1.55 ± 0.03
					<i>i</i>	1.6 ± 0.8	1.16 ± 0.12
					<i>l</i>	0.6 ± 0.3	0.3 ± 0.1
b	4.2	4.2	10.4 ^d	0.0 ± 0.2	<i>h</i>	5.8 ± 0.4	1.54 ± 0.03
					<i>i</i>	1.7 ± 0.3	1.13 ± 0.07
					<i>l</i>	1.2 ± 0.1 ⁵	0.27 ± 0.05
	40	4.2	10.4 ^d	-0.1 ± 0.2	<i>h</i>	4.6 ± 0.4 ⁵	1.59 ± 0.03
					<i>i</i>	1.5 ⁵ ± 0.4	1.23 ± 0.07
					<i>l</i>	0.7 ± 0.1	0.39 ± 0.06
	60	4.2	10.4 ^d	-0.4 ± 0.3	<i>h</i>	3.6 ± 0.3	1.56 ^c
					<i>i</i>	1.3 ± 0.2	1.18 ^c
					<i>l</i>	0.6 ⁵ ± 0.1	0.32 ^c
	80	4.2	10.4 ^d	-0.8 ± 0.5	<i>h</i>	1.7 ± 0.3	1.56 ^c
					<i>i</i>	0.7 ± 0.2	1.18 ^c
					<i>h</i>	1.2 ± 0.1 ⁵	1.56 ^c
	115	4.2	10.4 ^d	+1.5 ± 1.0	<i>h</i>	5.3 ± 0.8	1.55 ± 0.10
				Proposed values ($T=4.2$ K)	<i>i</i>	1.5 ± 0.7	1.16 ± 0.15
					<i>l</i>	1.0 ± 0.5	0.31 ± 0.10

^aValues given are for parameter choices $g_e/g_g = -3.74$ and $x=2.7$ (except proposed values in three bottom rows).

^bTotal intensity (sum of six lines) after background and linewidth correction.

^cFixed parameter (average of values from listed fits of 4.2- and 40-K spectra, obtained with source *b*).

^dFixed parameter (average of values from unlisted fits of 4.2- and 40-K spectra, obtained with source *b*).

respond to some parameter values at the limits of the allowed region (see figure caption).

In the bottom rows of Table I, proposed values for the hyperfine fields B_{hf} and relative intensities I_{rel} at liquid helium are given. The limits of error given to these values take into account the uncertainties in x and g_e . If an accurate value of g_e becomes available, the value of B_{hf}^h may be re-estimated and the new error would be reduced to about 20 kG.

In the column of Table I marked "Intensity," total absorption depths (summed for six lines) of the different components are given. These have been obtained by multiplying the background-corrected depths by Γ_m/Γ_0 , where Γ_m is the measured width (column 4 of Table I) and $\Gamma_0 = \Gamma_n(1 + 0.135 T_a)$, the width expected if there were only absorber thickness broadening¹⁴ ($\Gamma_n = 0.68$ mm/sec is the natural width of the 80-keV line, $T_a = \sigma_a f_a n_a = 0.72$ (4 K) or 0.51 (21 K) the reduced absorber thickness).

The absorption depths given in Table I will be used in Sec. IV to derive low-temperature recoilless fractions for the different components of the source spectra.

B. $FeTe^{125}$

Mössbauer spectra of the 35.6-keV γ transition in Te^{125} were measured both with a 400- μ Ci dif-fused $FeSb^{125}$ source and a 450- μ Ci implanted Fe^{125} source in combination with a 22-mg/cm² $ZnTe$ (enriched to 71% in Te^{125}) absorber. Sources 1 and 2 (see Table II) were mounted in a small permanent magnet producing a field of 420 G in the plane of the source foil. The magnet was fixed to the moving source rod. The transverse magnetic field serves to reduce uncertainties caused by possible differences of the magnetization of the Sb^{125} and I^{125} sources. The spectrum obtained with the $FeSb^{125}$ source is shown in Fig. 4. It can be fitted very well to a six-line pattern representing a single magnetic-field component.

The appearance of the spectrum is very similar to that of one component of the $FeXe^{131}$ spectrum (see Fig. 1). This is not surprising because the 80-keV transition in Xe^{131} and the 35.6-keV transitions in Te^{125} are both transitions between $\frac{3}{2}^+$ and $\frac{1}{2}^+$ shell-model states with opposite magnetic moments and similar magnetic-moment ratios.

In the fitting procedure of the spectrum obtained

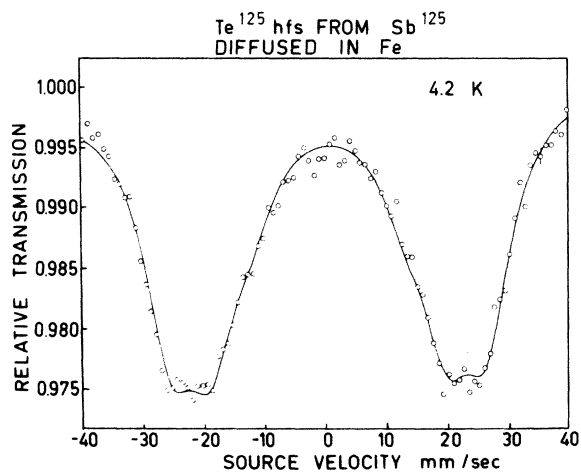


FIG. 4. Mössbauer spectrum obtained at 4.2 K with diffused $FeSb^{125}$ source and ZnTe absorber. The line drawn through the measured points represents a least-squares fit to a six-line pattern expected for one unique value of the magnetic hyperfine field $B_{hf} = 678$ kG.

with the $FeSb^{125}$ source, the hyperfine field B_{hf} , the absorption depth I_0 , the g_e/g_g , the isomer shift δ , and the value of x in the intensity ratios $3:x:1:1:x:3$ of the six lines of the spectrum were chosen as variable parameters. The fit yields $g_e/g_g = -0.21 \pm 0.01$, in good agreement with the value obtained by Frankel *et al.*¹⁵ and $x = 2.75 \pm 0.15$, the values of the other parameters are given in Table II. The quantity I_0 in this table is the total absorption depth (summed over the six lines) after correction by a factor 2.1 for the background under the 35.6-keV line that is caused by x rays and other γ lines.

The fit of the single-component $FeSb^{125}$ spectrum is used to facilitate the analysis of the more complex spectra obtained with the FeI^{125} source. These spectra, taken at 4.2 and at 78 K, are shown in Fig. 5. They contain at least two more components than the $FeSb^{125}$ spectrum, as is clear from Fig. 6 which gives the difference of the FeI^{125} spectrum and the properly normalized $FeSb^{125}$ spectrum. The form of the difference spectrum prompted us to fit the gross spectrum with the following three components: two six-line patterns for high- and intermediate-field fractions (h and i) and a third six-line pattern with a larger width of the individual lines, representing fractions of Te atom in sites with lower fields (l). The line-widths of components h and i are chosen equal. In the least-squares-fitting procedure all parameters are left free, except sometimes one of the line-widths which otherwise may tend to an unphysical value while there is no significant improvement of χ^2 . The intensity-ratio parameter x in the ratio $3:x:1:1:x:3$ was taken equal to that found for the

$FeSb^{125}$ source: $x = 2.75$. The drawn lines in Fig. 4 represent the fits thus achieved. The relevant parameters obtained from these fits are given in Table II. The quantity $I_0^{(h,i)}$ for the components h and i again is the total background-corrected absorption depth; for component l , $I_0^{(l)}$ is obtained by multiplying the absorption depth by the ratio Γ_l/Γ_0 of the widths of component l and the other two components.

In order to obtain more information about source magnetization, two spectra measured with the FeI^{125} source, one with the source in the transverse 420-G field, and the other outside were analyzed without using the intensity ratio parameter $x = 2.75$ obtained from the $FeSb^{125}$ spectrum as a fixed parameter. As expected, the fits are not very sensitive to the value of x and the errors therefore rather large: For the unmagnetized source we find $x = 2.4 \pm 0.3$ and for the magnetized source $x = 2.8 \pm 0.3$. A completely magnetized source in our geometry should yield $x = 3.7$. This shows that the transverse field of 420 G that we have used only produces a partial orientation of the magnetic mo-

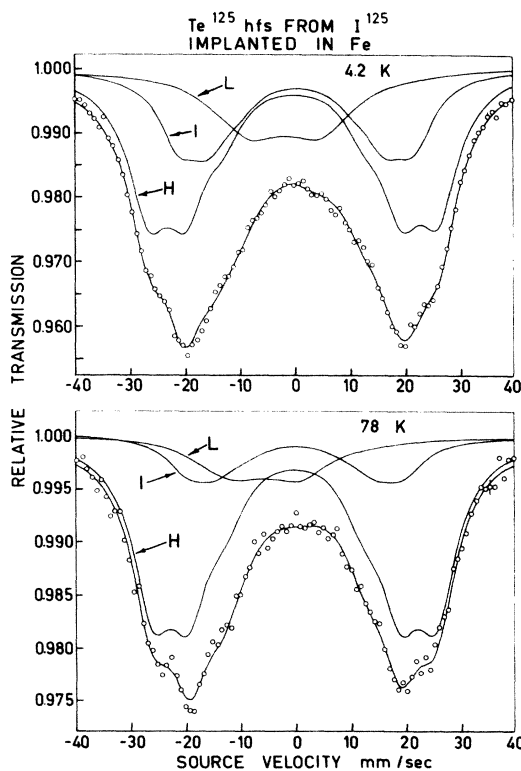


FIG. 5. Mössbauer spectra obtained with implanted FeI^{125} source and ZnTe absorber at 4.2 and at 78 K. The line drawn through the measured points represents a least-squares fit to a three-component model. Separate components are given by lines h (high field), i (intermediate field), and l (low field).

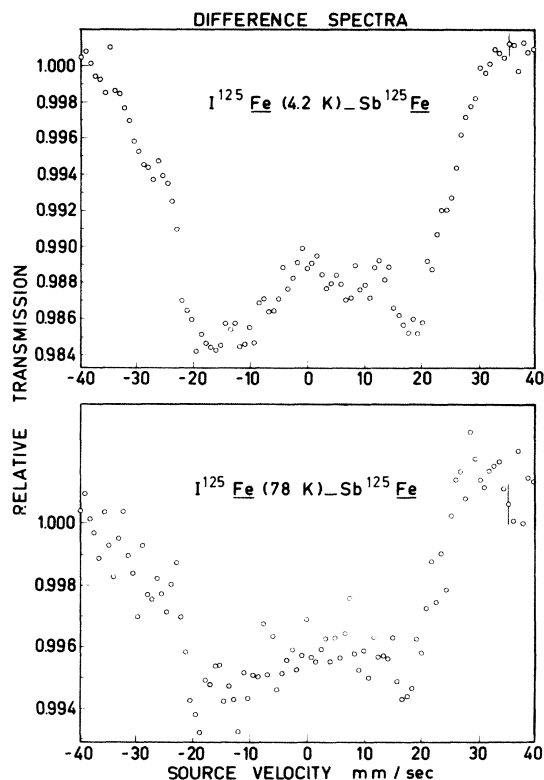


FIG. 6. Difference of Mössbauer spectra obtained with FeI^{125} and $FeSb^{125}$ sources at 4.2 and at 78 K. The normalization of the $FeSb^{125}$ spectrum was obtained from the three-component fits represented in Fig. 4 by the drawn lines.

ments of the iron near the impurity, even though the bulk magnetization of the foil is close to saturation.

IV. DISCUSSION AND INTERPRETATION OF RESULTS

A. Hyperfine fields

The values measured for the magnetic hyperfine fields of impurities with atomic numbers from 50 to 56 in iron are collected in Fig. 7. In some cases, high-, intermediate-, and low-field components (h , i , l) have been observed. The shaded region (labeled l) indicates the possible field range for the components l . The fields for Te and Xe were obtained in the investigations reported here, the other values were taken from a recent compilation.¹⁶

For the nonmagnetic impurities in the region considered, the hyperfine field is almost entirely due to the Fermi-contact interaction resulting from the net electron spin density at the nucleus. It can be expressed as

$$B_{hf} = \frac{8}{3} \pi \mu_B \{ |\psi_{\uparrow}(0)|^2 - |\psi_{\downarrow}(0)|^2 \}, \quad (1)$$

where $|\psi_{\uparrow(\downarrow)}(0)|^2$ is the density of the spin-up (-down) electrons at the nucleus, assumed to be constant over the nuclear volume. Because only s electrons contribute significantly, we will write $\psi = \psi_s$.

So far, there exists no theory that starts from first principles to calculate impurity hyperfine fields in ferromagnetic metals, but several models have been put forward to account for the observed trends of the fields. The first of these was originated by Daniel and Friedel¹⁷ and modified by Campbell.¹⁸ In these approaches, the effect of exchange-polarized conduction electrons, scattered from the impurity and setting up a screening charge around it, is considered. The impurity is represented by a square potential well. It has an effective ionic charge difference Z relative to the

TABLE II. Parameters obtained from Mössbauer spectra with $FeSb^{125}$ and FeI^{125} sources vs a $ZnTe^{125}$ absorber, using the 35.6-keV transition in Te^{125} .

Source and external field	Source and absorber temp (K)	Linewidth ^a (mm/sec)	Isomer shift (mm/sec)	Component	Intensity (I_0 , %)	Hyperfine field (B_{hf} , kG)
No. 1: $FeSb^{125}$ in 420 G	4.2	10.3 ± 0.5	0.4 ± 0.2	h	17.9 ± 1.3	678 ± 5
		9.0 ± 0.4	-0.1 ± 0.2	h	9.7 ± 0.5	690 ± 7
		9.0 ± 0.4	0.5 ± 0.2	i	4.9 ± 0.4	560 ± 20
No. 2: FeI^{125} in 420 G	78	15 ± 1.5	-1.9 ± 0.4	l	3.4 ± 0.4	200 ± 100
		9.1 ± 0.4	-0.4 ± 0.2	h	7.1 ± 0.4	674 ± 7
		9.1 ± 0.4	0.0 ± 0.5	i	1.4 ± 0.3	520 ± 30
No. 3: FeI^{125} no field	4.2	15 ^b	-5.7 ± 1.0	l	1.3 ± 0.2	190 ± 100
		9.2 ^b	0.4 ± 0.2	h	9.3 ± 0.5	692 ± 7
		9.2 ^b	0.5 ± 0.2	i	4.2 ± 0.3	540 ± 20
		15 ± 2	0.4 ± 0.3	l	2.4 ± 0.4	170 ± 100

^aNatural width 5.0 mm/sec.

^bFixed parameter.

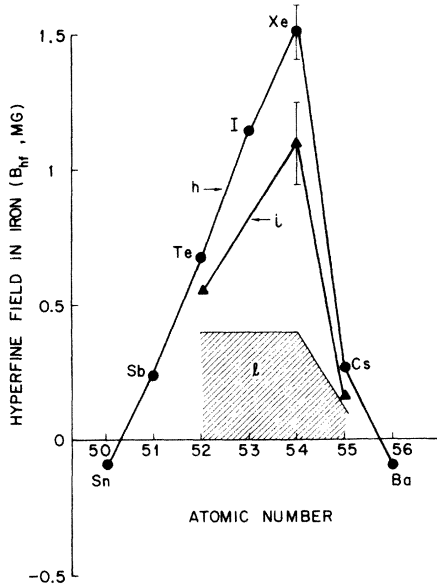


FIG. 7. Magnetic hyperfine fields of impurities with atomic numbers from 50 to 56 in iron. For Te, Xe, and Cs at least three different components (h , i , and l) of the field have been observed.

host ions that is compensated by the screening charge. The hf field at the impurity nucleus is calculated from the contact interaction of the screening electrons. Sign and magnitude of the field depend on the depth of the potential well, which in turn is determined by Z . Assuming (with Campbell) that the ionic cores of the host atoms carry a charge $Z_h = +1$, we must make an appropriate choice for the charge Z_i of the impurity core in order to fix the screening charge $Z = Z_i - Z_h$.

For the particular case of the noble-gas xenon, we may choose $Z_i = 0$ ($Z = -1$) or $Z_i = 8$ ($Z = 7$), depending on whether we attribute the eight electrons in the $5sp$ shell to the core or not. For both choices, Campbell's approach leads to small (or zero) hyperfine fields ($|B_{hf}| < 50$ kG), very different from the observed value of 1.5 MG. Qualitatively, this can be understood as follows: If $Z = -1$, the impurity acts as a potential chimney instead as a well, repelling rather than attracting a screening charge, while for $Z = 7$ the s -type states of the screening electrons lie well below the conduction band and are only slightly polarized. This conduction-electron polarization model, therefore, cannot account for the large positive hyperfine fields observed for impurities with filled (or almost filled) sp shells. Another approach toward understanding these fields was made by Shirley,¹⁹ who considered the direct polarization of impurity s orbitals due to their overlap with $3d$ orbitals of

the surrounding iron atoms (In the Daniel, Friedel, and Campbell models such interactions are not considered. Shirley, on the other hand, does not consider the contribution of the delocalized $4s$ electrons in the iron.) If overlap occurs, the s -type Xe wave functions must be hybridized with the $3d$ Fe wave functions of the same spin in order to maintain the orthogonality of the electron orbitals. Shirley restricted his calculations to Xe $5s$ orbitals. In that case the new normalized $5s$ spin-up wave function due to overlap with one spin-up $3d$ orbital is given by

$$\psi'_{5s\uparrow} = (1 - \langle 3d | 5s \rangle^2)^{-1/2} \times (\psi_{5s\uparrow} - \langle 3d | 5s \rangle \varphi_{3d}), \quad (2)$$

where $\langle 3d | 5s \rangle$ denotes the overlap integral. Due to the orthogonality of the spin functions, the spin-down wave function $\psi_{5s\downarrow}$ remains unchanged: $\psi'_{5s\downarrow} = \psi_{5s\downarrow} = \psi_{5s}$. Thus, a spin-up density excess

$$|\psi'_{5s\uparrow}(0)|^2 - |\psi_{5s}(0)|^2 \approx \langle 3d | 5s \rangle^2 |\psi_{5s}(0)|^2$$

per $3d$ electron results at the impurity nucleus. The $s-d$ overlap integral, however, is zero (due to the orthogonality of the orbital terms of the s and d wave functions) except for the $m_l = 0$ $3d$ electrons. Thus, the calculated matrix element comes entirely from the $3d$ electrons in the $m_l = 0$ state. Under $L-S$ coupling, one would expect the spin-up (or spin-down) electrons to be equally distributed among the five possible m_l states. The effective number of $3d$ spins producing the exchange is then only $\frac{1}{5}$ the net electronic spin polarization. According to Eq. (1) the contact hf field per $3d$ electron is $(\frac{8}{3}\pi)\mu_B |\psi_{5s}(0)|^2 \langle 3d | 5s \rangle^2$ and the total contact hf field due to the $5s$ shell is

$$B_{hf} = \frac{8}{3}\pi \mu_B |\psi_{5s}(0)|^2 \Delta n_{3d} \times \sum_i \langle 3d | 5s \rangle_i^2, \quad (3)$$

where the summation over the surrounding $3d$ electrons is replaced by a summation over the surrounding iron atoms and a multiplication with Δn_{3d} , the effective number of $3d$ electrons with spin up in one iron atom. For the case of a substitutional impurity the summation over nearest-neighbor iron atoms can be replaced simply by multiplication with a factor 8.

Shirley found $B_{hf}(FeXe) \approx 3$ MG, taking into account the relaxation of the iron lattice around the large Xe impurity. A possible effect of charge transfer due to covalent bonding is neglected. This appears to be a reasonable assumption for the case of a noble-gas impurity.

More complete overlap calculations for $FeXe$ were performed²⁰ by Hafemeister, and subsequently by Sondhi, who took into account all impurity s

shells. In this case, apart from squares of overlap integrals for the different shells, cross products between different shells appear in the expression for the hyperfine field. Since the cross products between shells with Δn odd are negative and rather large, the final result for the overlap field is reduced by a factor of about 2.3 relative to the value found if only $3d$ - $5s$ overlap is considered. The fields found from Hafemeister and Sondhi's calculations are $B_{\text{hf}}(\text{FeI}) = 0.10$ MG, $B_{\text{hf}}(\text{FeXe}) = 0.11$ MG; far smaller than those given by Shirley. Apart from the fact that Shirley did not take into account inner-shell contributions this discrepancy results from Shirley's considerably higher estimates of $|\psi_{5s}(0)|^2$ and $\langle 3d | 5s \rangle^2$ in Eq. (3).

There is at least one serious theoretical shortcoming in the overlap calculations just discussed, namely, the use of free-atom wave functions. There are good reasons to believe that the $3d$ electrons in iron metal are less localized than in a free atom, which would lead to an increase of the overlap integral. Also, the outer-shell s orbitals of the large xenon impurity are considerably modified in the small space available in the iron host, leading to an increase of the s density at the nucleus.

Finally, the exact amount of lattice relaxation around the impurity is unknown. This also has a large influence on the field: An increase of the Fe-Xe distances by 10% leads to a decrease in the overlap field by a factor of about 2. Further theoretical investigations are needed to clear up the large discrepancy between the overlap calculations and the experimental values.

According to Hafemeister and Sondhi's calculations the hf fields of impurities below xenon decrease with atomic number, but somewhat more slowly than the experimental values. The sudden drop of the field for cesium $B_{\text{hf}}(\text{FeCs}) = 0.18 \times B_{\text{hf}}(\text{FeXe})$ presents a special problem.

Shirley's overlap calculation yields a decrease of the field to only about 0.5 of the xenon field and Hafemeister²⁰ even reports a slight increase. An additional large negative contribution to the hyperfine field must be invoked to explain the small value of $B_{\text{hf}}(\text{FeCs})$. The conduction-electron polarization model does yield a negative contribution for this case ($Z_{\text{Cs}} = 1$, $Z_{\text{Fe}} = 1$, so $Z = 0$), but it is much too small: according to Campbell,¹⁸

$$B_{\text{hf}}^{\text{cep}} \approx -0.072 \times B_{6s}(\text{Cs}) \approx -150 \text{ kG},$$

if a free-atom value $B_{6s}(\text{Cs}) = 2.1$ MG is used for the contact field of one $6s$ electron. One may question, however, if this is correct since the space available for a substitutional cesium atom in the iron lattice is much smaller than that occupied by a free cesium atom. If charge neutrality is required within a Wigner-Seitz cell around the impurity, the screening charge must be confined to

a much smaller region than available for a $6s$ valence electron in a free atom. This would increase the screening charge density at the nucleus and hence the effective value of $B(\text{Cs})$. This idea is supported by the large value measured for the isomer shift of the 81-keV transition of Cs^{133} substitutionally imbedded in iron.²¹ This shift corresponds to an increase of contact charge density $\Delta\rho_s(0) \approx 2 \times 10^{26}/\text{cm}^3$ relative to a Cs^+ ion as compared to a free-atom $6s$ contact density $\rho_{6s}(0) = 2.6 \times 10^{25}/\text{cm}^3$. It can be shown that only a relatively small fraction of this large charge density increase is caused by the overlap distortion of the $5s$ orbitals. The major part must, therefore, be due to the screening charge. If we take into account that a part of the charge density increase $\Delta\rho_s(0)$ must be attributed to overlap effects, the contact density of the screening charge is estimated to be a factor 4-6 larger than that of a $6s$ electron in a free Cs atom. Assuming the same degree of polarization of the screening charge as Campbell, we then derive a 4-6 times larger negative value of the conduction-electron polarization contribution to the field: $B_{\text{hf}}^{\text{cep}} = -600$ to -900 kG. If we sum this with a positive-overlap-polarization contribution of the order of 1 MG, a total field in the range of the experimental value $B_{\text{hf}}(\text{FeCs}) = 273 \pm 10$ kG is obtained.

Our discussion so far has only been concerned with the field ascribed to purely substitutional impurities, i. e., impurities surrounded by a regular iron lattice. We now turn to the interpretation of the lower-field components observed in the Mössbauer spectra. In earlier work on the hyperfine interaction of Cs^{133} in iron, we have qualitatively interpreted these components as being due to impurity atoms associated with one or more vacancies.^{4,7} For the case of xenon in iron we may now place this interpretation on a somewhat more quantitative basis, if we assume the hyperfine field to be mainly due to overlap polarization. In order to do so, we must know (i) the Xe-Fe distances both for the pure substitutional case and for various Xe-vacancy clusters and (ii) the functional dependence of the overlap polarization on the Xe-Fe distance. The first item of information is obtained from lattice-relaxation calculations of Drentje and Ekster²² for α -iron containing small xenon-vacancy clusters. Their model is the same as used by Anderman and Gehman,²³ who made similar calculations for xenon-vacancy clusters in copper. Some of the clusters considered here are shown in Fig. 8. The nearest-neighbor (nn) Fe-Xe distance for a purely substitutional xenon atom is calculated as 2.70 Å, the next-nearest-neighbor (nnn) distance as 2.96 Å. In an undistorted lattice these distances would be $(\sqrt{3}/2)a = 2.48$ Å and $a = 2.68$ Å, respectively (a being the lattice constant of α -iron). In the xenon-

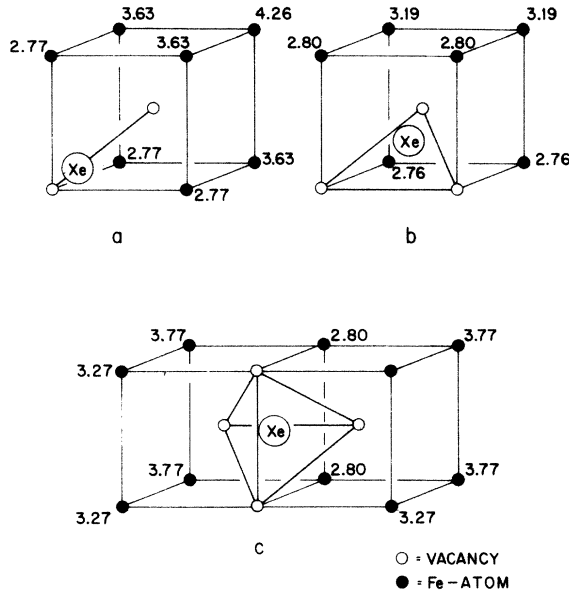


FIG. 8. Three xenon-vacancy clusters arising from the initial configuration of (a) Xe plus one nearest-neighbor vacancy; (b) Xe plus one nearest- and one next-nearest-neighbor vacancy; (c) Xe plus two nn and one nnn vacancy. Equilibrium positions reached by xenon atoms after lattice relaxation are indicated. Iron atoms are indicated at their positions in an unrelaxed lattice. Numbers near iron atoms give distances between these atoms in the relaxed lattice and the xenon atom (in Å).

vacancy clusters both the xenon atom and the surrounding iron atoms relax from their initial positions. Some of the relaxed Xe-Fe distances are indicated in Fig. 8. We shall only take into account contributions to the hyperfine field of the nearest-neighbor (nn) and next-nearest neighbor (nnn) iron atoms; those of higher-order neighbors turn out to be quite small. Further restricting ourselves to $3d$ - $5s$ overlap we may write for the hyperfine field [see Eq. (3)]

$$B_{\text{hf}}^{\text{ov}} = \frac{8}{3} \pi \mu_B \Delta n_{3d} |\psi_{5s}(0)|^2 \sum_i S_i^2, \quad (4)$$

where $S_i = \langle 3d | 5s \rangle_i$ denotes the overlap integral per spin-up $3d$ electron with the i th iron atom. The summation is carried out over nn and nnn neighbors. $|\psi_{5s}(0)|^2$ is the contact density at the Xe nucleus of one atomic $5s$ electron. Hafemeister has shown²⁴ that overlap integrals for small overlaps can be approximated very well by

$$S_i(r_i) = S(r_0) e^{-(r_i - r_0)/\rho}. \quad (5)$$

In our case, r_i is the distance between a xenon impurity and the i th-neighboring iron atom. The value of the characteristic distance ρ depends on the particular overlapping orbitals, but in most cases not very strongly. Hafemeister gives, for instance,

the following values of ρ for some s , d overlap integrals: Cu($3d$, $4s$), $\rho = 0.45$ Å; Ag($4d$, $5s$), $\rho = 0.43$ Å; Au($5d$, $6s$), $\rho = 0.44$ Å. For $5s$, $5s$ overlap in xenon he finds $\rho = 0.52$ Å. Shirley finds a field-vs-distance dependence for the $3d$, $5s$ overlap of Fe-Xe pairs that corresponds to $\rho = 0.52$ Å. Using this value of ρ and Drentje and Ekster's relaxed values of r_i we have calculated the ratio of the sums $\sum S_i^2$ for some xenon-vacancy clusters and the sum $\sum S_{i0}^2$ for a purely substitutional xenon atom in a relaxed lattice. The results are compared in Table III with the measured ratios $B_{\text{hf}}^{(i)}/B_{\text{hf}}^{(h)}$ and $B_{\text{hf}}^{(i)}/B_{\text{hf}}^{(h)}$ for FeXe^{131} . The experimental ratios for FeTe^{125} are also given in the table, but a comparison with the calculations has limited validity since the interatomic distances for the Xe-vacancy clusters were used in those calculations.

The hf field ratios calculated from this model suggest that the intermediate-field component is due to an impurity associated with one nearest-neighbor vacancy, while the low-field component probably is a sum of contributions of impurity atoms associated with at least two vacancies. Most of the ratios of squares of overlap-integral sums given in Table III were found to be remarkably insensitive to the value of the parameter ρ in Eq. (5). If we double this value ($\rho = 0.88$ Å) the ratios change as follows: cluster 1, $0.80 \rightarrow 0.79$; cluster 2, $0.96 \rightarrow 0.94$; cluster 3, $0.41 \rightarrow 0.44$, cluster 4, $0.22 \rightarrow 0.33$. For this reason, the calculated hf field ratios also do not depend sensitively on the absolute values of the interatomic distances.

It should be noted that we have excluded from the start the existence of interstitial sites for the Xe atoms. We feel justified in doing so on the basis of the results of channeling measurements⁸ on xenon implanted in iron, that do not give evidence for the existence of such sites.

B. Comparison with other results

The results on implanted I^{125} and I^{131} sources reported here and other recent work mentioned in connection with these results show a complex behavior for these systems; it is useful to reexamine

TABLE III. Comparison of hyperfine-field-component ratios for FeXe and FeTe with squares of overlap-integral sum ratios for some xenon-vacancy clusters.

Cluster	$\sum S_i^2 / \sum S_{i0}^2$	$B_{\text{hf}}^{(i)} / B_{\text{hf}}^{(h)}$	
		FeXe	FeTe
1. subs. imp. -1 nn vac.	0.80	0.72 ± 0.1	0.80 ± 0.04
2. subs. imp. -1 nnn vac.	0.96		
3. subs. imp. -1 nn vac. -1 nnn vac.	0.41	0.2 ± 0.07	0.30 ± 0.15
4. subs. imp. +2 nn vac. +1 nnn vac.	0.22		

older work in this light.

The value first published for the hf field of Xe in Fe, $B_{\text{hf}}(\text{FeXe}) = 1.01 \pm 0.04$ MG, for example, was derived from a nuclear-orientation measurement,^{25,26} using implanted FeXe^{133} sources, under the assumption that all of the implanted Xe ions were in equivalent sites. Niesen²⁶ later analyzed the original measurement in terms of two sites, one in which the hf field is large and another in which it is too small to lead to any significant nuclear orientation. For a fractional population of the high-field sites in the range 0.5–0.75 he found a field in the range 1.2–1.6 MG.

Recently, Pattijn *et al.*²⁷ investigated the nuclear orientation of $\text{Xe}^{131\text{m}}$ and $\text{Xe}^{133\text{m}}$ implanted in iron. They measured the (strong) anisotropy of the M4 γ transitions from the isomeric transitions in the temperature range 11–100 mK. Using the same simplifying assumption as Niesen, viz., one high-field and one low-field fraction, they fitted their data with a high-field value $B^{(h)}$ and a high-field fraction a_h as adjustable parameters and found $B_{\text{hf}}^{(h)}(\text{FeXe}) = 1.51 \pm 0.16$ MG and a_h in the range 0.4–0.7 depending on the particular source used.

Both of these analyses are consistent with our new results as well as with the channeling results of Feldman and Murnick.⁸ From their location experiments it is known that approximately 50% of the implanted ions are in substitutional sites, with the remainder in uncharacterized nonsubstitutional sites. The results are also consistent with those obtained from Mössbauer spectra of the 81-keV transition in Cs^{133} obtained with implanted FeXe^{133} sources,^{4,7} which showed a high-field site containing $(40 \pm 5)\%$ of the Cs ions. It is clear that the existence of an intermediate-field site cannot be concluded from the nuclear-orientation results, since a two-site model already gives a satisfactory fit to the data. In this respect the Mössbauer measurements allow a further differentiation; for none of the cases studied (FeI^{125} , FeI^{131} , and FeXe^{133}) does a two-site model give a satisfactory fit of the spectra.

C. Recoilless fractions and site population

The relative populations a_j of the impurity sites are related to the intensities I_j and recoilless frac-

tions f_j of the different components by

$$a_j = (I_j / f_j) / \sum (I_j / f_j). \quad (6)$$

The intensities are given in Tables I (FeXe^{131}) and II (FeTe^{125}); in order to determine the populations a_j we must inquire first what information can be obtained from these measurements about the recoilless fractions.

For FeTe^{125} , measurements were carried out at 4.2 and 78 K. The line intensities for the intermediate- and low-field components decrease faster with temperature than those for the high-field component. This suggests a lower Debye temperature for the lower-field components. If we assume that the temperature dependence of the recoilless fractions is sufficiently well given by a Debye-Waller factor, we can derive low-temperature recoilless fractions for the source from the intensity ratios of the different components at 78 and 4.2 K. In order to do this, the intensities given in Table II must be corrected for the difference in temperature of the ZnTe^{125} absorber. Using the value $\Theta = 180$ °K measured by Blattner *et al.*²⁸ for the characteristic temperature of ZnTe, and the known absorber thickness and Te^{125} resonance cross section, we find that the resonant absorption increases from 0.71 at 78 K to 0.79 at 4.2 K. The corrected source component intensities for 78 and 4.2 K and their ratios I_T/I_0 are given in Table IV. From these ratios characteristic temperatures of the different components are derived by solving for $z = \Theta/T$ the equation

$$I_T/I_0 = \exp[-(\frac{3}{2}E_r/k\Theta)P(z)], \quad (7)$$

with

$$P(z) = 1 + (4/z^2) \int_0^z [x dx / (e^x - 1)],$$

inserting $T = 78$ K and $E_r = 5.44 \times 10^{-3}$ eV. The values of Θ thus found are given in column 5, the low-temperature recoilless fractions $f_0 = e^{-(3/2)E_r/k\Theta}$ in column 6, and the site populations, given by Eq. (6), in column 7 of Table IV. It is interesting to note that these site populations are about the same as those found earlier⁴ for FeXe^{133} sources (see

TABLE IV. Parameters obtained from Mössbauer spectra of a FeI^{125} source and used for calculation of site populations.

Component	Intensity (\mathcal{I} , %)		Int. ratio ^a $I_{78}/I_{4.2}$	Charact. temp. Θ (K)	Recoilless fraction f_0 at $T=0$	Site
	78 K	4.2 K				population a (%)
<i>h</i>	7.1 ± 0.4	9.7 ± 0.5	0.81 ± 0.10	250_{-40}^{+70}	0.68 ± 0.04	46 ± 5
<i>i</i>	1.4 ± 0.3	4.9 ± 0.4	0.33 ± 0.05	135 ± 10	0.50 ± 0.02	32 ± 4
<i>l</i>	1.3 ± 0.2	3.4 ± 0.4	0.42 ± 0.08	145 ± 15	0.52 ± 0.03	22 ± 6

^aAbsorption corrected for different absorber temperature.

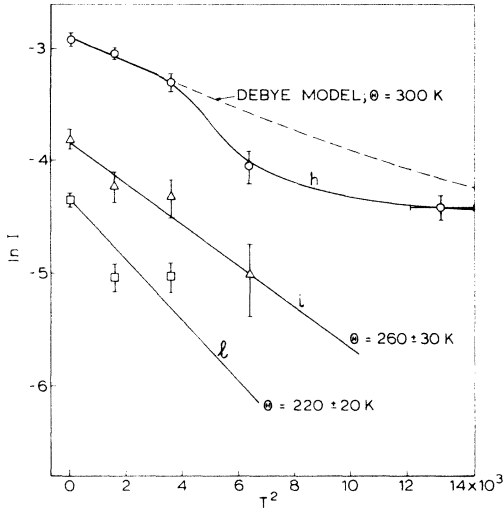


FIG. 9. Plots of the logarithm of the recoilless fraction vs the square of the source temperature for high (h), intermediate (i), and low-field (l) components of Mössbauer spectra obtained with an FeI^{131} source. Drawn lines: fits for components i and l , assuming Debye-Waller-factor temperature dependence. Broken line: Debye-Waller-factor dependence of recoilless fraction for a characteristic temperature $\Theta_h = 300$ K derived from the measured low-temperature recoilless fraction of the high-field component.

also Table VI).

The characteristic temperature of the pure substitutional site agrees with the expectation based on Lipkin's rule²⁹:

$$\Theta = \Theta_{Fe}(m_{Fe}/m_{Xe})^{1/2} \approx 300 \text{ K.}$$

This rule is valid if the force constant between an impurity atom and a host atom is the same as that between two host atoms. The lower characteristic temperatures for the lower-field sites ($\Theta \sim 200$ K) indicate smaller force constants or increased space for the impurity. These observations are in agreement with the hypothesis that the impurity in the lower-field sites is associated with vacancies.

For the case of $FeXe^{131}$, where results are available at a number of different source temperatures (see Table I), a more complete analysis in terms of Debye-Waller factors should be possible, but unfortunately the accuracy of the results turns out not to be quite satisfactory. At temperatures well below the Debye temperature, Eq. (7) can be approximated by³⁰

$$\ln(I_T/I_0) = \ln[f(T)] + \text{const} \\ = -\frac{3}{2}(E_r/k\Theta)\left[1 + \frac{2}{3}\pi^2(T/\Theta)^2\right]. \quad (8)$$

This suggests a linear dependence between $\ln I_T$ and T^2 . Plots of $\ln I_T$ vs T^2 are shown in Fig. 9 for each of the three spectral components h ,

i and l , using the data for Table I. We have fitted components i and l with straight lines, from which Debye temperatures $\Theta_i = 260 \pm 30$ K and $\Theta_l = 220 \pm 20$ K and low-temperature recoilless fractions $f_i(0) = 0.17 \pm 0.04$ and $f_l(0) = 0.12 \pm 0.03$ follow.

The high-field component, however, shows a markedly nonlinear behavior: It does not obey a Debye model. This deviation is probably due to a strong anharmonicity of the motion of the large Xe atom in a substitutional position. Therefore, we do not trust the value $\Theta = 300$ K derived from a Debye-model fit to the lowest three points (see Fig. 9). In itself, the peculiar behavior of the recoilless fraction of the substitutional xenon is interesting, but it complicates our task of finding the low-temperature recoilless fraction $f_h(0)$ for the high-field component. This quantity can be derived in principle by using the estimate of the recoilless fractions of the other components. We may write for the background- and linewidth-corrected low-temperature intensities I_{0j} ($j = h, i, l$) of the three components, given in Table I:

$$I_{0j} = a_j f_j(0) \left[1 - e^{-T_a/2} J_0\left(\frac{1}{2} T_a\right)\right] \\ = a_j f_j(0) \tau_a. \quad (9)$$

Using the value

$$T_a = n_a \sigma_a f_a = 0.72 \pm 0.10$$

derived in Sec. IIA for the absorber at $T = 4.2$ K, we find $\tau_a = 0.28 \pm 0.03$. We have calculated the relative site populations a_i and a_l , using the proposed values of I_{0j} in Table I (bottom). Since $a_h + a_i + a_l = 1$, we also find a_h and $f_h(0)$. The results, collected in Table V, are not very accurate, due to the large errors in the intensities of the three components of the Mössbauer spectra. Within their limits of error, the site populations agree with the more accurate ones derived from the FeI^{125} spectra. The recoilless fraction $f_h(0) = 0.48 \pm 0.24$ can be related to a characteristic temperature

$$\Theta_h = -\frac{3}{2} E_r / k \ln f_h(0) = 620_{-320}^{+750} \text{ K.}$$

A somewhat more accurate estimate of this characteristic temperature may be obtained if we assume the site populations for the FeI^{131} sources to be the same as those for the FeI^{125} sources. Inserting the value $a_h = 0.46 \pm 0.05$ obtained for the $I^{125}Fe$ source (see Table IV) into Eq. (9) we find $f_h = 0.41 \pm 0.08$ and $\Theta_h = 510 \pm 120$ K. This value is higher than the one that follows from the Debye model as well as that expected according to Lipkin's rule.²⁹ This indicates that the low-temperature Xe-Fe force constant is much larger than the Fe-Fe force constant, which points to a large compression of the xenon atom in the substitutional

TABLE V. Low-temperature recoilless fractions and site populations for implanted FeI^{131} sources.

	$f(0)$	a
h	0.48 ± 0.24	0.39 ± 0.20
i	0.17 ± 0.04	0.31 ± 0.14
l	0.12 ± 0.03	0.30 ± 0.15

site. The atomic volume of a xenon atom is about $6 \times$ the volume of an iron atom in the iron lattice. For the Te impurity discussed before, where Lipkin's rule works well, the volume excess is only a factor of about 1.5. The smaller values of Θ for the intermediate- and low-field sites again indicate that the available space has increased, consistent with vacancy association.

In Table VI, some of the results obtained in this and earlier investigations for Sb, Te, I, and Cs impurities in iron are reviewed. While Sb implants^{1,2} and Te implants^{3,4} yield unique hyperfine fields, I and Xe implants clearly do not. This striking difference can be attributed to the change in size of the impurities. According to Flynn³¹ Sb and Te are imbedded as neutral atoms in a metal with a conduction-electron density like that found in iron. The highly electronegative iodine, however, forms I^- ions. If this is true, the atomic (ionic) radius jumps from about 1.6 Å for Sb and Te to 2.2 Å for I^- and Xe. The process of site formation can now be described as follows: When an impurity comes to rest at a substitutional position in the lattice it has just created several vacancies and interstitials by collisions near the end of its track. Some of the vacancies are trapped by the impurities, while others may be annihilated by interstitials or form stable clusters. If the implanted atom is large, the trapped vacancies cannot be annihilated by interstitials because the "binding energy" of the vacancy to the impurity exceeds the annihilation energy. For the smaller impurities, the annihilation energy may exceed the binding energy so that vacancies initially present close to

the impurity are annealed, leaving the impurity atom in a pure substitutional site.

The requirement of a small size, however, does not always seem to be sufficient for obtaining pure substitutional implants: Rare-earth ions implanted in iron, which are believed to be in a 3^+ ionic state, certainly have a small enough ionic radius ($R = 0.93 - 1.11$ Å). Yet, channeling measurements^{32,33} yield a substitutional fraction of only about 50% for the case of Yb implanted in iron ($R = 0.94$ Å). The different character of rare-earth implants on the one hand and the Sb and Te implants on the other, might be connected with their different electronegativities; further investigations will be needed to clear up the different substitutionality.

Finally, some remarks are in order about the assumption made so far that the impurity location is not affected by the β decay. The recoil energies imparted to the implanted atom are 0.1 eV for the $I^{125} - Te^{125}$ capture decay and at most 3.2 eV for the $I^{131} - Xe^{131}$ β decay. These energies are certainly too small to displace the daughter nuclei if the parent iodine nuclei were imbedded in the normal lattice of some iodine compound. It may be questioned, however, if in the thermodynamically highly unstable situation encountered here, a much smaller amount of energy could suffice to cause a displacement. An indication that the relative site populations of parent and daughter impurities are about the same is obtained from recent nuclear orientation experiments with sources of I^{131} implanted in iron, performed by Koene and Postma.³⁴ These authors analyze their results for the degree of orientation of the I^{131} nuclei, obtained from the anisotropy of the γ rays emitted in their decay, in terms of a two-component model for the hyperfine field acting on the I^{131} nuclei. It is assumed that a fraction a_0 of the nuclei experience the full hyperfine field, and a fraction $a_1 = 1 - a_0$, zero hyperfine field. As an average for various sources a value $a_0 \approx 0.6$ is found. The authors have also analyzed their measurements using our results for the site populations: $a_h = 0.4$ (high field, $B_{hf} = B_{hf}^{(h)}$),

TABLE VI. Summary of hyperfine fields and site populations obtained for Te, I, Xe, and Cs impurities in iron.

Source	Mössbauer line		Fields (kG)				Site occupation (%)	
	keV	Impurity	h	i	l	h	i	l
1% $FeSb^{125}$	35.6	Te^{125}	678 ± 5	100
$10^{15}/cm^2 FeI^{125}$	35.6	Te^{125}	685 ± 5	540 ± 15	190 ± 60	46 ± 5	32 ± 4	22 ± 6
$10^{15}/cm^2 FeTe^{129m}$	27.7	I^{129}	1150 ± 15	100
$3 \times 10^{14}/cm^2 FeI^{131}$	80	Xe^{131}	1550 ± 100	1160 ± 100	300 ± 100	39 ± 20	31 ± 14	30 ± 15
$10^{14}/cm^2 FeXe^{133}$	81	Cs^{133}	273 ± 3	130 ± 10	< 30	40 ± 5	20 ± 5	40 ± 10

$a_i = 0.2$ (intermediate field, $B_{\text{hf}} = 0.8 B_{\text{hf}}^{(h)}$), and $a_i = 0.4$ (low field, $B_{\text{hf}} \sim 0.2 B_{\text{hf}}^{(h)}$) and find a reasonable agreement with their experimental value of the gamma ray anisotropy.

V. CONCLUSIONS

Mössbauer spectra of γ transitions excited in the decay of implanted sources of I^{125} ($\rightarrow \text{Te}^{125}$) and I^{131} ($\rightarrow \text{Xe}^{131}$) in iron show that the implanted iodine atoms occupy at least three different nonequivalent sites in the iron lattice. As in previous measurements on sources of Xe^{133} implanted in iron,^{4,7} high-, intermediate-, and low-field components are observed in the Mössbauer spectrum. The new results can again be interpreted by assuming that the high-field component corresponds to substitutional impurities while the intermediate- and low-field components correspond to impurities associated with one or more vacancies. Apparently, the method of ion implantation makes it possible to obtain dilute solutions of elements that are at least partly substitutional for cases where the usual methods of alloying or diffusing fail, due to insolubility or chemical reactivity of the element concerned with respect to the host. From the Mössbauer spectra, reliable values can be obtained for the hyperfine fields of the high-field (substitutional) and intermediate-field components. A consistent semiquantitative interpretation for the hyperfine-field ratios between pure and damage sites can be given for both FeXe^{131} and FeI^{125} . The

high sensitivity of the hyperfine-field values to vacancy trapping opens important possibilities for radiation-damage annealing studies.

The high low-temperature recoilless fraction $f_h(0) = 0.41 \pm 0.08$ of the substitutional impurities indicates a substantial increase of the Xe-Fe force constant as compared with the Fe-Fe force constant. Probably, this can be ascribed to a strong compression of the large Xe atoms in the iron lattice. This interpretation is supported by the anomalous temperature dependence of the recoilless fraction of Xe in Fe.

Thus, the thermodynamically highly unstable systems that can be produced by ion implantation appear to have some unique and interesting properties, worthy of further investigation.

ACKNOWLEDGMENTS

The investigation reported here has been made possible by the intensive use of the Groningen radioactive isotope separator operated by T. Klootsema. The contributions of N. S. Wolmarans in the early stages of the FeI^{125} investigation are gratefully acknowledged. The authors wish to thank K. W. West for running the FeI^{131} experiments and W. E. Falconer and W. A. Sunder for making available the sodium-perxenate absorber material. They are indebted to I. Sondhi for permission to cite her results before publication. One of them (H. de Waard) gratefully acknowledges the excellent working conditions at Bell Laboratories.

*On leave from the University of Groningen, Groningen, Netherlands.

¹H. R. Andrews, J. F. Knott, F. M. Pipkin, and D. Santry, *Physics Lett. A* **26**, 58 (1967).

²P. G. E. Reid, M. Sott, N. J. Stone, D. Spanjaard, and H. Bernas, in *Hyperfine Structure and Nuclear Radiations*, edited by E. Matthias and D. A. Shirley (North-Holland, Amsterdam, 1968), p. 719.

³H. de Waard, J. Heberle, P. J. Schurer, H. Hasper, and F. W. J. Koks, in *Hyperfine Structure and Nuclear Radiations*, edited by E. Matthias and D. A. Shirley (North-Holland, Amsterdam, 1968), p. 331.

⁴H. de Waard, *Mössbauer Spectroscopy and its Applications* (IAEA, Vienna, 1972), p. 123.

⁵R. B. Alexander, N. J. Stone, D. V. Morgan, and J. M. Poate, in *Hyperfine Interactions in Excited Nuclei*, edited by G. Goldring and R. Kalish (Gordon and Breach, London, 1971), p. 229.

⁶A high substitutional fraction was found for $6 \times 10^{14} \text{ cm}^{-2}$ 100-keV implants of Te in Fe by L. C. Feldman and H. de Waard, in *Applications of Ion Beams to Metals*, edited by S. T. Picraux, E. P. EerNisse, and F. L. Vook (Plenum, New York, 1974), p. 317.

⁷H. de Waard, P. Schurer, P. Inia, L. Niesen, and Y. K. Agarwal, in *Hyperfine Interactions in Excited Nuclei*, edited by G. Goldring and R. Kalish (Gordon and Breach, London, 1971), p. 89.

⁸L. C. Feldman and D. E. Murnick, *Phys. Rev. B* **5**, 1 (1972).

⁹G. J. Perlow, in *Chemical Applications of the Mössbauer Effect*, edited by V. I. Goldanskii and R. H. Herber (Academic, New York, 1968), p. 377 and references given in that chapter.

¹⁰G. J. Perlow, *Phys. Rev.* **135**, B1102 (1964).

¹¹J. Hauck, *Z. Naturforsch. B* **25**, 226 (1970).

¹²S. Margulies and J. R. Ehrman, *Nucl. Instrum. Methods* **12**, 131 (1961).

¹³N. S. Wolmarans and H. de Waard, *Phys. Rev. C* **6**, 228 (1972).

¹⁴D. A. O'Connor, *Nucl. Instrum. Methods* **21** (1963) 318.

¹⁵R. B. Frankel, J. J. Huntzicker, D. A. Shirley, and N. J. Stone, *Phys. Lett. A* **26**, 452 (1968).

¹⁶T. A. Koster and D. A. Shirley, in *Hyperfine Interactions in Excited Nuclei*, edited by G. Goldring and R. Kalish (Gordon and Breach, London, 1971), p. 1239.

¹⁷F. Daniel and J. Friedel, *J. Phys. Chem. Solids* **24**, 1601 (1963).

¹⁸I. A. Campbell, *J. Phys. C* **2**, 1338 (1969).

¹⁹D. A. Shirley, *Phys. Lett. A* **25**, 129 (1967).

²⁰D. W. Hafemeister (unpublished). Similar calculations have been carried out by I. Sondhi (unpublished).

²¹H. de Waard and S. A. Drentje, *Proc. R. Soc. (Lond.) A* **311**, 139 (1969).

²²S. A. Drentje and J. Ekster, *J. Appl. Phys.* (to be

- published).
- ²³A. Anderman and W. G. Gehman, *Phys. Status Solidi* 30, 283 (1968).
- ²⁴D. W. Hafemeister, *J. Phys. Chem. Solids* 30, 117 (1967).
- ²⁵L. Niesen, J. Lubbers, H. Postma, H. de Waard, and S. A. Drentje, *Phys. Lett. B* 24, 144 (1967).
- ²⁶L. Niesen, thesis (Leyden, Netherlands, 1971) (unpublished).
- ²⁷H. Pattijn, R. Coussement, G. Dumont, E. Schoeters, R. E. Silverans, and L. Vanneste, *Phys. Lett. A* 45, 121 (1973).
- ²⁸R. J. Blattner, L. K. Walford, and T. O. Baldwin, *J. Appl. Phys.* 43, 935 (1972).
- ²⁹H. J. Lipkin, *Ann. Phys. (N.Y.)* 23, 28 (1963).
- ³⁰R. H. Nussbaum, B. G. Howards, W. L. Nees, and C. F. Steen, *Phys. Rev.* 173, 653 (1968).
- ³¹C. P. Flynn, *Phys. Lett. A* 41, 45 (1972).
- ³²F. Abel, M. Bruneaux, C. Cohen, H. Bernas, J. Chaument, and L. Thome, *Solid State Commun.* 13, 113 (1973).
- ³³R. B. Alexander, E. J. Ansaldo, B. I. Deutch, L. C. Feldman, and J. Gellert in Ref. 6, p. 365.
- ³⁴B. K. S. Koene and H. Postma, *Nucl. Phys. A* 219, 563 (1974).